A GENERALIZED APPROACH TO MODELING THE INTEGRATED EFFECTS OF RATCHETTING IN FUEL RODS

D.C. COLEMAN, P.E. MacDONALD
Nuclear Fuel Services Inc., Rockville, Maryland 20852, U.S.A.

SUMMARY

Differential thermal expansion, fuel swelling, cladding creep-down, and pellet cocking and jamming are all potential occasions for fuel-cladding mechanical interference. In light of possible detrimental effects resulting from extensive mechanical interactions, it is important to include in the scope of an overall fuel rod performance analysis those mechanisms which pertain to the ratchetting phenomenon and its effect on the dimensional behavior of interacting fuel and cladding systems.

A fuel rod ratchetting model and supporting data are described in which radial and axial deflections occur over fuel and cladding length increments where mechanical interactions have taken place. Two concepts were developed: 1) a local "effective gap" which incorporates localized pellet cracking and cocked pellet locking effects and 2) an "interaction length", defined as an axial segment of the rod where the effective gap at the top and bottom becomes negative. Appropriate allowances are made to account for fuel and cladding restructuring and accompanying stress relaxation in both the axial and radial (effective gap) directions.

Six miniature differential transformers were used to measure cladding elongation at power in the Halden Boiling Water Reactor. Comparisons of measured and calculated early life cladding elongations are shown for rods of various fuel densities and inital gaps. Favorable agreement for three successive full power cycles over a period of about 260 hours demonstrates the applicability of general assumptions consistent with a macroscopic treatment of the mechanisms involved and their cumulative effect on overall fuel rod dimensional behavior.

I. INTRODUCTION

Differential thermal expansion, fuel swelling, cladding creep-down, pellet cocking and cracked pellet jamming are all potential occasions for fuel-cladding mechanical interference. When sufficient locking conditions are met in the course of power cycling operation, portions of the fuel stack expanding under thermally induced forces result in biaxial compressive forces on the fuel and tensile forces on the cladding. In this dynamic situation, stress levels continually seek equilibrium by some combination of radial and axial deformation of both fuel and cladding. If the latter consequence always predominates, plastic strain in the cladding may eventually result in a life-limiting situation for the fuel pin. On the other hand, if excessive or uncontrolled fuel relocation or densification occurs, unacceptable power peaking, increased cladding collapse propensity, or additional non-uniform mechanical effects may be the result. It is important for these reasons then to include in the scope of an overall fuel rod performance analysis those mechanisms which pertain to the ratchetting phenomenon and its effect on the dimensional behavior of interacting fuel and cladding systems.

II. EXPERIMENTAL RESULTS

In November 1971, Nuclear Fuel Services, Inc. (NFS), began a systematic study of a number of fuel design parameters in the Halden Boiling Water Reactor. A range of instruments was chosen which allows for an accurate monitoring of overall assembly performance as well as the dynamic mechanical and thermal behavior of individual fuel elements during irradiation.

The rods in the first test assembly, IFA-226, are instrumented with five diaphragm type rod internal pressure sensors, six miniature differential transformers for cladding elongation measurement, and four tungsten/tungsten-rhenium fuel centerline thermocouples. A turbine flow meter and two coolant thermocouples are mounted in the assembly inlet and outlet respectively. Eight self-powered beta current neutron detectors monitor radial and axial flux distributions.

The readings from all instruments are recorded every 15 minutes. Local power is calculated for each elongation sensor reading using the neutron detector output and suitable calibration constants determined from the thermal and hydraulic instrumentation. In determining the power history of each test rod, variations in pellet dimensions, fuel density, enrichment, and radial and axial flux distributions are also considered.

The fuel is mixed oxide, pressed and sintered pellets clad in Zircaloy-4. The rods were fabricated at NFS's Erwin Tennessee plant with plutonium generated at the Consumers Power Company's Big Rock Point Reactor and separated in NFS's West Valley, New York reprocessing facility. The range of fuel densities and diametral gaps in the six rods equipped with elongation sensors are typical of current commercial designs and highly characterized prior to irradiation. The length, density, and diameter of every pellet was measured and recorded. After sorting, rods with various exact combinations of fuel density and pellet-to-cladding gap were constructed. Cladding dimensions were measured with respect to the location of individual pellets. The following table provides pertinent pre-irradiation dimensional data:

FUEL ROD CHARACTERISTICS

Rod Identification	Diametral Gap (μm)	Diametral Gap (mils)	Pellet O.D. (mm)	Pellet O.D. (in)	Geometric Density (% T.D.)
AH	91.4	3.6	9.401	.3701	94.5
AJ	139.7	5.5	9.355	.3683	94.4
AK*	200.7	7.9	9.312	.3666	96.0
AM	198.1	7.8	9.304	.3663	94.5
AO*	210.8	8.3	9.304	.3663	92.1

Active fuel length 607mm
Pellet length (dished) 15.2 mm
Plenum length 178 mm
Clad Thickness 0.617 mm

Initial plenum pressure - 1 atm
Fill gas - Helium
Enrichment - 9.2% PuO_2
*Rods with center thermocouple.

The irradiation of IFA-226 thus provides an opportunity to measure axial cladding deflections in typical individual test rods during normal reactor operation including full power cycling. Early life operation represents a situation where, with minimal fuel swelling and fission gas release, the cumulative effects of basic thermal fuel-cladding interaction mechanisms are directly reflected in the data.

Since local power and fuel temperature measurements are also being made, the highly instrumented nature of the test assembly allows for a more thorough understanding of interrelated effects due to spatially dependent thermal expansion differences resulting from flux peaking in individual pins. The verification of NFS's thermal models by favorable comparions of measured and predicted fuel temperatures using IFA-226 and other data permit the analytical evaluation of the general ratchetting mechanism in terms of the initially temperature dependent phenomena.

Figure 1 shows initial power ramp elongation data as a function of the rod peak linear heat rating. Gap and density are shown to have respective effects on the power level at which interaction begins and the rate of elongation after this point. In all cases the nominal hot gap is not calculated to have closed in the range of peak powers experienced by the rods, but nonetheless, the existence of mechanical interference is obvious.

In reality, even the low heat ratings at the very beginning of the power ramp induce fuel cracking and non-uniform pellet relocations which combine to minimize the effective gap available for accommodating hot fuel. Pellet cocking and jamming is especially enhanced in the first cycle where the fuel and cladding systems have been the least tempered by a demanding thermal environment.

Subsequent power cycling causes additional mechanical interaction but the data suggests more uniform behavior as shown for example by Figure 2. Fuel and cladding plasticity at high heat loads, during the preceding power cycles has acted to relax mechanical interaction stresses and acclimate both materials to spatial restrictions. The transition between cladding thermal expansion alone and additional deflections caused by mechanical interaction becomes more defined and occurs at power levels more consistent with the closing of a nominal hot gap.

Figure 3 shows typical as built diametral gap variation in one of the elongation sensor rods. Even though tight (Pellet O.D. $\pm$ .0005 in, Clad I.D. $\pm$ .001 in, and end face offset .0015 in) dimensional control was maintained during test rod fabrication, worst case behavior is likely at those axial locations near the top of the fuel stack where construction of the radial void volume during power cycling is aggravated by the largest axial displacement contributions from the fuel below.

III. GENERALIZED RATCHETTING MODEL

The results of a fuel rod ratchetting model were compared with the data. In the method, radial and axial deflections occur over finite fuel and cladding length increments where fuel cladding mechanical interactions are calculated to exist. In subroutine form, the model is adaptable to an overall fuel rod performance analysis where reasonable confidence already exists as to the validity of calculated radial and axial temperature distributions and the material properties of both fuel and cladding.

Two key concepts, pertaining to an "effective gap" and an "interaction length" were developed, the use of which permitted the ratchetting mechanism to be modeled more in terms of experimentally founded physical assumptions than on the basis of analytically rigorous extensions of single node theory. The notion of effective gap was introduced in order to account for an increased tendency for mechanical interaction in rods where pellet cracking and cocked pellet locking effectively reduces clearances between fuel and cladding at selected axial locations. Interaction lengths were defined as those finite lengths of UO_2 pellets, moving under swelling or thermally induced forces, which are locked to the cladding at top and bottom due to closure of the effective gap. The overall axial deformation of the fuel and cladding are determined by integrating the effects of dimensional changes that have occurred in individual interaction lengths over the course of a finite duration constant power step. Within a power step, appropriate allowances are made to account for fuel and cladding restructuring and accompanying stress relaxation in both the axial (interaction length) and radial (effective gap) directions.

Efforts to determine the onset of mechanical interaction in new rods include the fact that fuel cracking and "built-in" parameters such as diametral gap and end face non-perpendicularity variances within individual pins result in earlier interaction than what would be expected using nominal gaps. But nominally determined diametral clearances are nonetheless significant. In a fuel performance analysis based on a series of constant power time intervals, these gaps represent uniform dimensional changes and pellet relocations and are used for heat conduction calculations. On a macroscopic scale, these calculations in turn represent thermal mechanisms largely unaffected by localized mechanical conditions. If good comparisons of measured and calculated fuel temperatures are obtained by analytical methods which assume uniform strains, then predictions for the onset of mechanical interaction need only account for additional gap penalties associated with pellet cocking and jamming. Added gap penalties result in an effective gap which, after sufficient creep of the fuel rod material during ratchetting at high temperatures, gradually approaches the nominal "heat flow" gap.

Whenever the effective gap is less than zero, an interference fit is assumed to exist at that axial location. The magnitude of the contract pressure, p, is determined from the condition that the increase in the inner radius of the cladding plus the decrease in pellet radius must be equal to the effective gap, δ. Using the thick-walled cylinder theory developed by Timoshenko [1]:

$$p = \frac{\delta \; E_p \; E \; (K^2-1)}{Ea \; (1-\mu_p) \; (K^2-1) + E_p R_i (1-\mu + K^2(1+\mu))} \qquad (1)$$

where E_p, μ_p, and a are the pellet Young's Modulus, Poisson's Ratio and radius; E, μ, and R_i are the cladding Young's Modulus, Poisson's Ratio and inside radius; and K is the ratio of the cladding outside radius to inside radius. If the fuel and cladding deflections due to all other contributions (thermal expansion, swelling, and hydrostatic forces) have already been determined prior to this point, P is actually the contact pressure P_{ct}, which can then be included in calculating the total effective stress in the radial direction, σ_e:

$$\sigma_e = \frac{\sqrt{3}\ (1+K^2)(P_i+P_{ct}) - 2\ K^2 P_o}{2\ (K^2 - 1)} \qquad (2)$$

where P_i and P_o are the internal and external (system) hydrostatic pressures respectively. The effective compressive stress on the pellet is adjusted at each radial location a_i in proportion to ratio a/a_i.

The problem of calculating subsequent axial deformations of the fuel and cladding as a result of this interference situation becomes one of keeping track of their relative length changes over that portion of the rod which is in a mechanically stressed condition. For this reason, predictions of fuel and cladding response at operating temperatures and under the added loading imposed by fuel-cladding interaction necessitates an accurate accounting of in-pile UO_2 and Zircaloy plasticity. The cladding creep rate for the subject analysis was based on the formulation of Ibrahim {2}. Ibrahim's equations were modified to account for observed, fast flux induced creep acceleration along the lines suggested by Watkins and Wood {3}.

A review of available data on the subject of in-pile ceramic oxide plasticity indicated that UO_2 creep behavior can be approximated by an equation of the form:

$$\dot{\varepsilon} = (C_1/((C_2 + D)\ G^2))\ \sigma\ \exp(C_3/T) + (C_4/(C_5 + D))\ \sigma^{4.5} \exp\ (C_6/T) + \sigma\ f \exp\ (C_7 \ln f - C_8) \qquad (3)$$

where $\dot{\varepsilon}$ is the steady state uranium dioxide creep rate, σ is the applied stress, T is temperature, f is fission rate, D is the fuel theoretical density, G is the UO_2 grain size and C_1, C_2, etc. are constants. The thermal creep component is based on a compilation of out-of-pile data and is similar to the creep correlation reported by Bohaboy et.al.{4}. The fission induced component is based on an understanding of UO_2 creep being accentuated under in-pile conditions because of high local temperatures experienced in the vicinity of fission events. Results of in-pile creep tests suggest that even at low power levels and bulk fuel temperatures, macroscopic deformations occur in operating fuel as a result of cumulative high temperature plasticity mechanisms taking place on a microscopic level. Therefore, the last term of equation 3 follows the general form suggested Solomon et.al.{5}.

A pellet with some finite non-perpendicularity between the end-face and outer surface, will be constrained by the cladding when the effective mechanical diametral gap, g_e, is less than zero. Over some length of fuel rod, the effective gap is related to the nominal, thermal, or mean gap by

$$g_e = \bar{g} - s\ \frac{\ell}{d} \qquad (4)$$

where $\bar{g}$ is the nominal hot diametral gap, s is the cold end face non-perpendicularity, and ℓ/d is the pellet cold length to diameter ratio.

D 1/

Considering non-uniform axial movements of a system of discontinuous segments, fuel jamming is encouraged when there is more space available to accommodate initial rotations of cracked pellet segments. For this case

$$g_e = \bar{g} - (s + \beta)\frac{\ell}{d} \tag{5}$$

where β is an empirical gap penalty variable which is related to the original free volume as follows:

$$\beta = A(g_c) + B \tag{6}$$

where g_c is the initial cold diametral gap and A and B are constants deduced from initial observed interactions in operating rods.

As discussed above, previous fuel-cladding interactions result in restructuring of both materials, the result being an equilibrium orientation at the lowest attainable stress. Thus, for a given axial station of the rod, the effective gap presented in equation 5 is a minimum value only at the onset of mechanical interaction. At the end of each time interval, the effective gap is determined as follows:

$$g_e = \bar{g} - (s + \beta)\frac{\ell}{d} + \epsilon_{f_i} d_f + \epsilon_{c_i} d_c \tag{7}$$

where ϵ_{f_i} is the fuel creep, d_f is the nominal hot and swelled pellet diameter, ϵ_{c_i} is the cladding creep, d_c is the nominal hot and elastically strained cladding inside diameter, and increasing i denotes increasing time. In equation 7 ϵ_{f_i} and ϵ_{c_i} include the generalized stress resulting from an interference fit based on an effective gap calculated at the beginning of the time interval as well as the net pressure difference.

In the analysis, the pellets are radially divided into 10 equal area rings. Ceramic oxide data indicates that fuel creep rates are significantly enhanced above ∿2600°F. Since the peripheral, lower temperature regions of fuel are to an extent creep resistant, they have been assumed to provide structural support. A contributing mechanism in the analysis is a radial fuel density distribution which is assumed to develop as a result of plastic compression of the material.

For axial deflections, when a portion of the rod is in a mechanically stressed condition, relative length changes of fuel and cladding are based on axial stress levels as determined from a total thermal strain potential ΔL_{fc}. During mechanical interaction over a single interaction length, L, the axial deflection of the fuel and cladding together, ΔL_{fc} is, of course, the sum of their individual displacements ΔL_c and ΔL_f. It follows that:

$$\Delta L_{fc} = FL\left[(/A_c E_c) + (1/A_f E_f)\right] \tag{8}$$

or:

$$\sigma_c = \Delta L_{fc} / \left\{A_c L\left[(1/A_c E_c) + (1/A_f E_f)\right]\right\} \tag{9}$$

$$\sigma_f = \Delta L_{fc} / \left\{A_f L\left[(1/A_c E_c) + (1/A_f E_f)\right]\right\} \tag{10}$$

where σ, A and E refer to axial stress, axial load bearing surface, and Young's Modulus of the fuel and cladding and F is the axial force.

The strain potential, ΔL_{fc}, is based on the difference in fuel and cladding lengths between the onset of interaction and the current values, including differences in plastic strains as well as thermal expansions. When an axial interaction length includes more than

one calculational increment as defined in the main program, the total strain potential is a cumulative amount which is equally divided among the increments.

As in the pellet radial creep calculation, where a bridging annulus does not extend into the fuel beyond the point where temperatures exceed 2600°F, the axial load bearing area of the pellet is similarly temperature dependent. For axial creep however, dimensional changes in the colder regions of the fuel are not determined by creep rates in the bridging annulus. Neither are they determined by peripheral relocation per se. Instead, given a competing mechanism where temperatures near the fuel surface support the pellet while interior temperatures between the surface and the limiting bridging annulus weaken the pellet (especially for cocked pellets), it has been assumed that some intermediate or average value determines the creep rate.

In summary, within the framework described, the following simplified situation has been modeled.

A) For each axial increment, at the beginning and the end of the current power step, the main program calculates:

- Fuel and cladding material properties and geometry
- Fuel and cladding temperatures
- Internal and external pressures on the cladding
- Fuel swelling
- Nominal hot gap

B) At the end of the previous power level the following information is stored:

- Effective gap from end of previous power level which reflects radial restructuring of the cocked or jammed pellets
- Cold length which reflects any previous plastic deformation

C) With this information, the following is generated in the ratchetting subprogram over the course of a current power level:

- If at the beginning of the current power level interference exists at an axial segment, an interaction length is defined and the radial pelled-cladding contact force is calculated
- Pellet and cladding creep radially at the interaction point, over the current power step, in response to stresses including pressure deflection (stresses are adjusted during small creep steps to allow for relaxation due to restructuring)
- The pellet jamming (effective gap) is adjusted and stored
- The axial differential fuel-cladding thermal expansions over a given interaction length between the time of pellet-cladding interaction (jamming) and the present are used to calculate axial tensile forces on cladding and compressive forces on fuel; deformation can occur over any number of interaction lengths.
- Fuel and cladding materials creep in small steps until the end of the current power level
- Elastic and plastic components of fuel and cladding deformation during the current power level are added to the cold cladding and fuel lengths from the end of the previous power level to calculate the current hot lengths
- The hot and cold cladding and fuel lengths are summed for all axial increments to get current total rod and stack lengths

IV ANALYTICAL RESULTS

Figure 4 shows an example of measured rod elongation for the startup ramp along with calculated values obtained using the model described; both as a function of rod peak power. Figure 5 presents the same comparison of measured and calculated values for the same rod

over the second full power cycle. Both data and predictions are consistent with the interrelated mechanisms alluded to previously

The data for rod AH suggested some additional interactions at very low power. Fabrication records for rod AH indicated that, due to the minimal gap size, interference between the fuel stack and the cladding was detected while the pellets were being loaded.

Agreement between data and calculation for the first few power ramps was found to be most favorable for rod AK. Fabrication records indicated that as built gap variation within the individual pins was smallest for rod AK. Therefore this data was most amenable to an analytical prediction in which the initial cold gap variation over the active length was not modeled, nominal values having been used in all cases.

Figure 6 shows an example of initial ramp elongation data and predictions as a function of time. The calculated onset of mechanical interaction does not include the second order effects of pellet slipping seen in the data prior to the initiation of pellet-cladding locking. For all cases, the slope of the calculated rod length change with respect to time shows favorable agreement with the measurements. Of special interest is the slope of fuel rod shortening between about 11 and 21 hours (real time axis). The axial stress, fuel temperature, and fission enhanced fuel creep models are generally supported by the dimensional consistency shown in the analytical results during this period of full power operation.

Figures 7 through 11 present data and calculated results for all of the subject rods over a larger time period. Both data and predictions also reflect the relative creep properties of UO_2 with respect to density. This effect is seen in comparing the results for rod AO (92.1%, 8.3 mils) with those of rod AK (96.0%, 7.9 mils). For the low density case, fuel stack shortening is significantly enhanced at the higher power levels encountered. A true comparison between the measured and calculated permanent cladding strain can be seen at the end of the power history when, due to a slow scram, the reactor power was essentially zero. The agreement is favorable in all cases even in light of

a) the previously mentioned additional jamming effects evidenced in rod AH
b) analytical conservatism with respect to fuel creep in low density rod AO
c) the fact that due to a limitation as to the number of steps used to describe the analytical power history, the choice of calculating points was arbitrary and in retrospect, not the optimum one.

IV CONCLUSIONS

Pellet cocking and cracked pellet jamming are apparent mechanisms for fuel-cladding mechanical interference and locking at relatively low power levels. In the course of power cycling operation, thermally induced fuel stack expansion results in axial compressive forces on the fuel and tensile forces on the cladding. Stress levels continually seek equilibrium by some combination of radial and axial deformation of both fuel and cladding.

A generalized ratchetting model was developed based on the concept of (1) and "effective gap" which includes localized pellet cracking and cocked pellet locking effects and (2) and "interaction length" defined as an axial segment where the top and bottom of the fuel stack is locked to the cladding over a given period of time.

Comparison of predictions with measured rod length changes for three successive full power cycles over a period of about 260 hours demonstrated the applicability of the general assumptions described.

REFERENCES

{1} Timoshenko, S., Strength of Materials - Part II, Advanced Theory and Problems, D. Von Nostrand Co., Princeton, New Jersey (1958).

{2} Ibrahim, E. F., An Equation for Creep of Cold Worked Zircaloy Pressure Tube Material, Report AECL 2582 (1965).

{3} Watkins, B., and Wood, D. S., "The Significance of Irradiation-Induced Creep on Reactor Performance of a Zircaloy-2 Pressure Tube", in Applications Related Phenomena in Zirconium and It's Alloys, American Society for Testing and Materials, Pennsylvania, Pennsylvania (1969).

{4} Bohaboy, P. E., Samoto, R. R., Conti, A. E., Compressive Creep Characteristics of Stoichiometric Uranium Dioxide, Report GEAP-10054 (1969).

{5} Solomon, A. A., Routbort, J. L., Voglewede, J. C., Fission Induced Creep of UO_2 and its significance to Fuel Element Performance, Report ANL-7857 (1971).

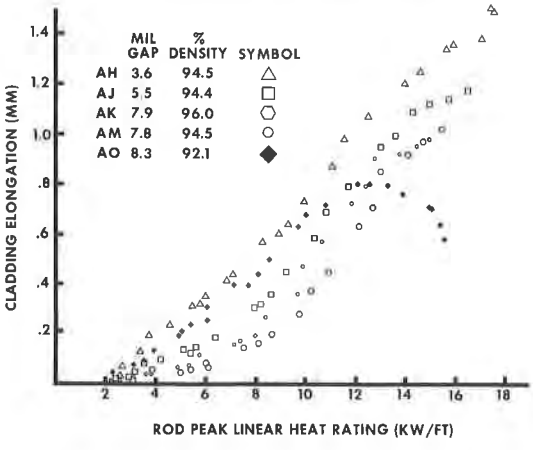

FIGURE 1

ROD ELONGATION VS ROD PEAK POWER

ZERO BURNUP

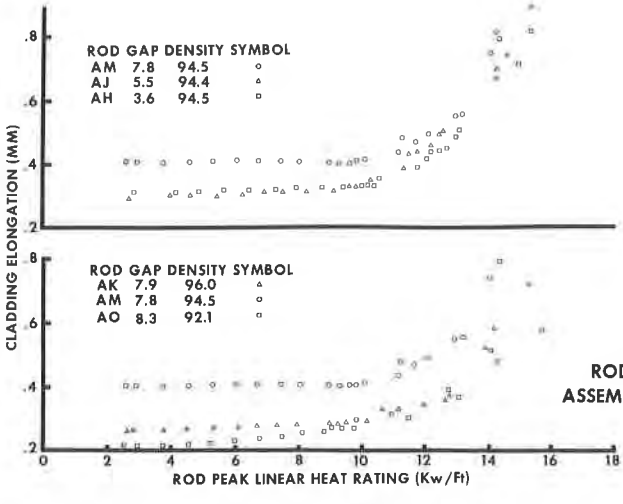

FIGURE 2

ROD ELONGATION VS ROD PEAK POWER

ASSEMBLY AVERAGE BURNUP 2000 MWD/MTM

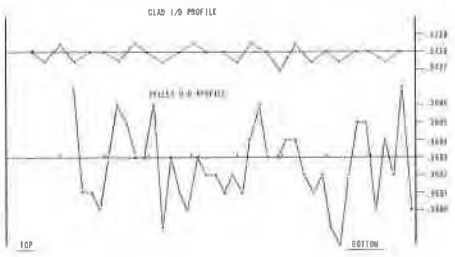

FIGURE 3

ROD AJ
DIMENSIONAL MEASUREMENTS

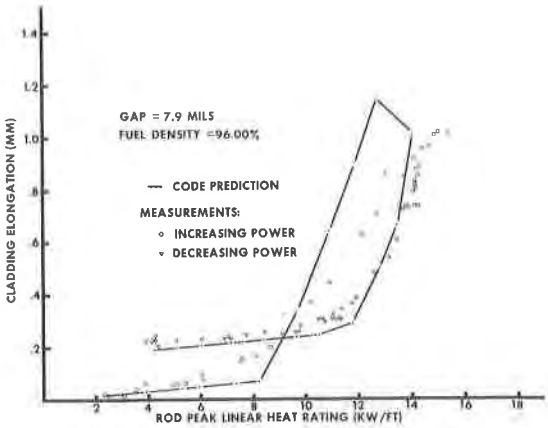

FIGURE 4

IFA - 226 ROD AK
ROD ELONGATION VS ROD PEAK POWER

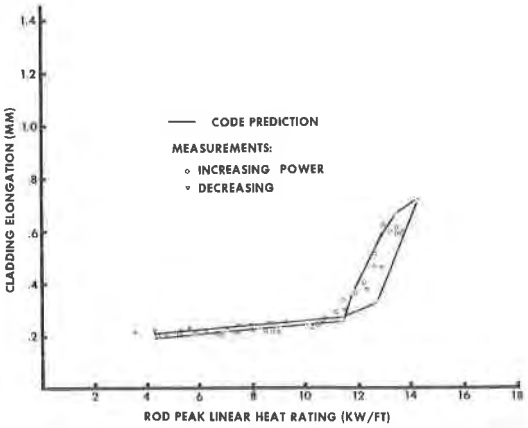

FIGURE 5

IFA - 226 ROD AK
ROD ELONGATION VS ROD PEAK POWER

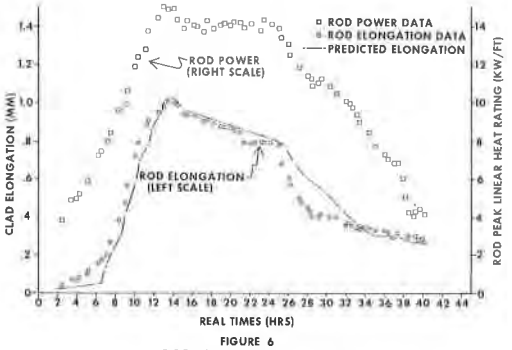

FIGURE 6
ROD ELONGATION VS TIME
IFA-226 ROD AM-FIRST POWER CYCLE

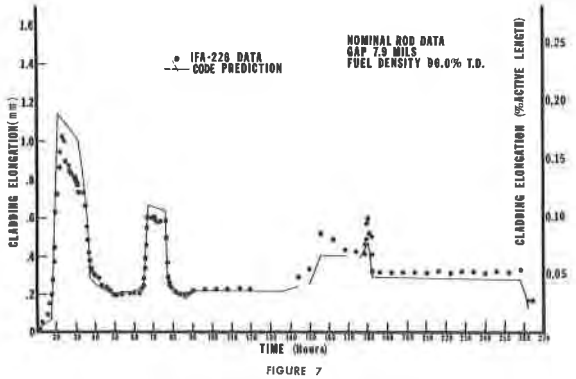

FIGURE 7
CLADDING ELONGATION vs. TIME (ROD-AK)

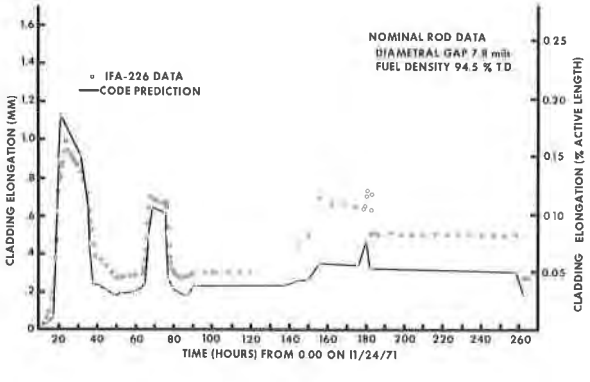

FIGURE 8
CLADDING ELONGATION VS. TIME - ROD AM

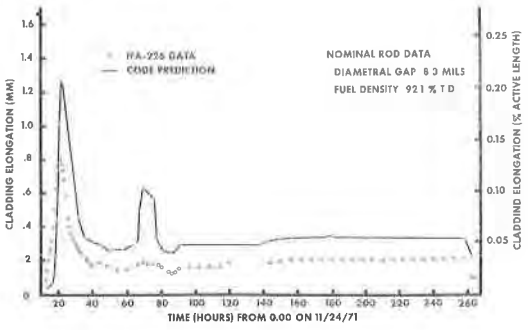

FIGURE 9

CLADDING ELONGATION VS. TIME - ROD AO

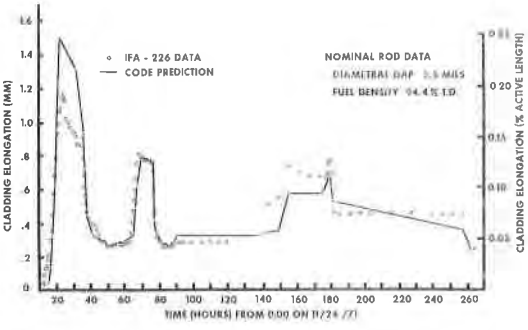

FIGURE 10

CLADDING ELONGATION VS. TIME - ROD AJ

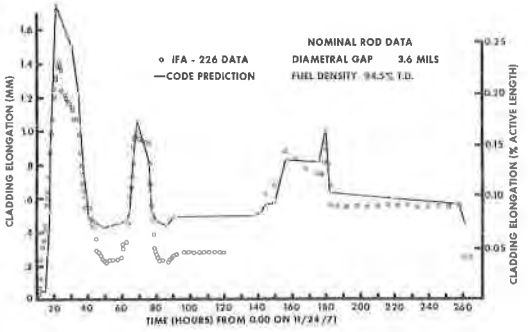

FIGURE 11

CLADDING ELONGATION VS. TIME - ROD AH